Astron. Astrophys. 117, 21–32 (1983)

ASTRONOMY AND ASTROPHYSICS

Empirical NLTE Analyses of Solar Spectral Lines

IV. The Fe I Curve of Growth

R. J. Rutten and C. Zwaan

Sterrewacht "Sonnenborgh", The Astronomical Institute, Zonnenburg 2, 3512 NL Utrecht, The Netherlands

Received July 15, accepted September 9, 1982

Summary. We present a solar curve of growth (Fig. 4a) for 991 Fe I lines, based on the NLTE modeling of the solar Fe I spectrum by Athay and Lites (1972) and Lites (1973) and on the best oscillator strengths now available. We show that neglect of the NLTE ionization departures affects the whole curve of growth appreciably; however, we confirm the result of the preceding paper of this series that neglecting Fe I NLTE departures can be largely corrected by assuming an NLTE-masking atmospheric model such as the Holweger and Müller (1974) photosphere.

We also present theoretical NLTE curves of growth, and we discuss their splitting due to wavelength dependency, differences in NLTE excitation, and variation in collisional damping. Comparison of the observed and theoretical curves of growth shows, however, that these forkings are largely hidden by noise in the equivalent width values of Moore et al. (1966).

We derive and discuss a new value of the solar iron abundance: $N_{Fe}/N_H=(4.7\pm0.5)10^{-5}$.

Key words: stellar photospheres – solar abundances – curve of growth – line formation – iron lines

I. Introduction

In the preceding paper of this series (Rutten and Kostik, 1982; henceforth Paper III) the effects of the departures from LTE on the core intensities of solar Fe I lines were discussed. In this paper we concentrate on the effects on equivalent widths, as exhibited by the curve of growth. Our goal is not to study NLTE departures, which is better done through modeling line profiles, but to set a solar example to stellar usage of the curve of growth by discussing its inherent spread and splits. We are thus concerned with the effects on the curve of growth of departures from LTE in the ionization and excitation equilibria, of wavelength dependency, and of variation in collisional damping. The curve of growth is used here to supply a survey of Fe I line formation for many lines simultaneously.

The most recent comparable studies of the solar Fe I curve of growth are those by Yamashita (1972) and Foy (1972). They use essentially the same laboratory and solar data, and both employ the opacity normalization tables of Cayrel and Jugaku (1963). Their results for the solar Fe I abundance and microturbulence, assumed height-independent, differ slightly (respectively, by 0.1 dex and 0.5 km s^{-1}); but there is larger difference in their conclusions on the collisional damping. Both authors emphasize the presence of large variation in the collisional damping and the subsequent spread in the curve of growth, which was pointed out earlier by Pagel (1965) and explained by Warner (1967) as variation in the mean square radii of Fe I orbitals. Foy so initiated the Meudon school of applying damping-split curves of growth in differential analyses (e.g. Cayrel et al., 1977). However, while Yamashita compares the observed damping values per line with predictions based on Warner's (1969) atomic radii and finds that van der Waals broadening represents them well, Foy argues that this is not so, and adds the surprising conclusion that the collisional damping varies strongly even between members of a single multiplet. His underlying assumption is that only damping affects the damping part of the curve of growth, and thus that any variations between strong lines have to be assigned to this parameter.

We conclude that it is of interest to study the line-by-line variation in the Fe I curve of growth. In particular, we propose to question whether variations within multiplets can be re-assigned to differences in NLTE excitation, which should indeed, if present, vary within multiplets with the oscillator strength. We base the construction of the curve of growth on the NLTE modeling of the solar Fe I spectrum by Lites (1972, 1973), following the conclusions from Paper III that the weaker Fe I lines agree well with Lites' strong-line fits, and that the conflicting success of the LTE description in fact supports his NLTE results equally well.

We describe the input data in Sect. II and the NLTE construction and the resulting curve of growth in Sect. III. In Sect. IV we present theoretical curves of growth, which we subtract from the empirical one to obtain scatter diagrams discussed in Sect. V. In Sect. VI we discuss the solar iron abundance.

II. Input Data

a) Oscillator Strengths and Line Strengths

For the atomic input data we use two complementary sets of transition probabilities. The first are the extremely precise furnace measurements of the oscillator strengths of low-excitation Fe I lines published by the Oxford group (Blackwell et al., 1979, 1980, 1982), henceforth called "Oxford" values. The second are the empirical oscillator strengths of medium-strong visual Fe I lines published by Gurtovenko and Kostik (1981), henceforth called

Send offprint requests to: R. J. Rutten

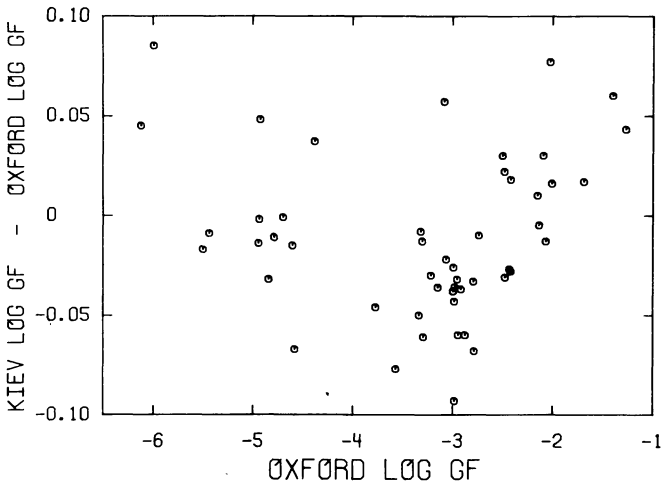

Fig. 1. Comparison of oscillator strengths for 50 lines of overlap

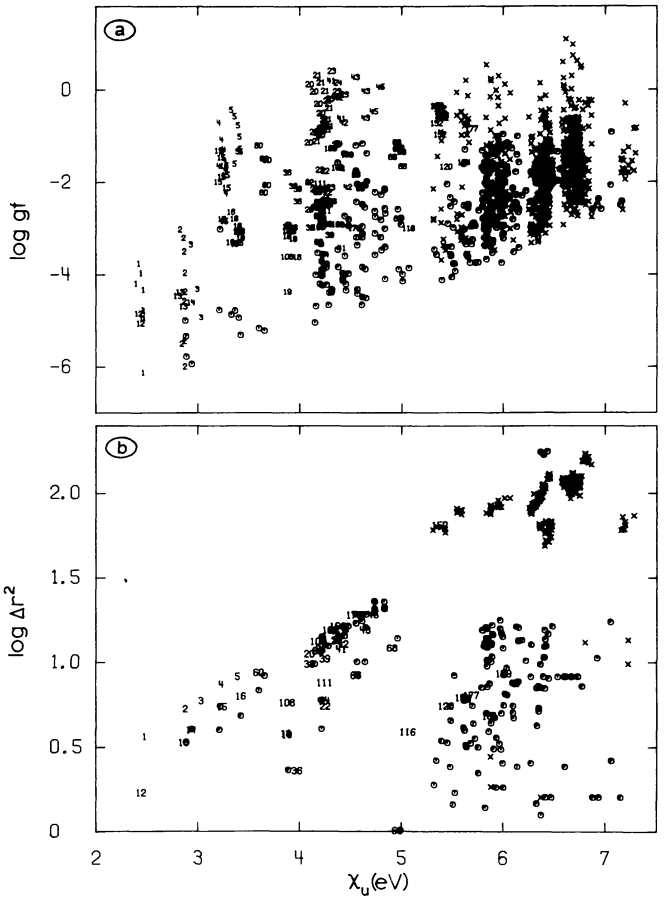

Fig. 2a and b. Input data to this study. **a** The logarithm of the oscillator strength against upper-level excitation energy χ_u, for 808 Kiev lines and 183 Oxford lines. Crosses are Kiev lines with upper levels of even parity, circles are Kiev lines with upper levels of odd parity, numbers are the multiplet designations of the Oxford lines, which all have upper levels of odd parity. **b** The logarithm of the difference in square atomic radii (atomic units) between upper and lower level against upper-level excitation energy χ_u, shown per multiplet with similar notation as in **a**

"Kiev" values. These are based on LTE fits of the central intensities of solar disk-center profiles, and have been normalized by Gurtovenko and Kostik to agree with the Oxford absolute scale for some lines of overlap. A subset of the Kiev values are the "$\dot{g}f_d$" values used in Paper III, where it is shown that they are quite reliable, except for the strongest lines of high excitation energy. The reason for this reliability is that the LTE fits are based on the LTE atmospheric model by Holweger and Müller (1974, henceforth HOLMUL). This model corrects implicitly for the neglected Fe I NLTE departures to a large extent.

For the observational input data we follow Yamashita (1972) and Foy (1972) and use the "reduced" equivalent widths W/λ, where W is the equivalent width and λ the wavelength, tabulated by Moore et al. (1970, henceforth MMH; Column 3, here multiplied by 10^{-6}).

After deletion of the Oxford lines without MMH equivalent width, of the Oxford lines withdrawn by Blackwell et al. (1982), and of the Kiev lines without MMH multiplet identification, there remain 183 Oxford lines and 860 Kiev lines, of which 52 lines are present in both sets. The differences between the two sets for 50 lines of overlap are shown in Fig. 1. The remaining two lines have exceedingly large loggf differences (-0.23 for λ499.41 and -0.87 for λ772.32); their Kiev values are probably wrong because these give deviating points in the curve of growth. Figure 1 confirms the good quality of the Kiev oscillator strengths; note that the vertical scale is expanded tenfold compared with the similar difference plots published by the Oxford group for other sets of oscillator strengths. We have deleted the lines of overlap from the Kiev list.

Our input sample thus consists of 183 Oxford lines and 808 Kiev lines. The two sets are largely complementary; together, they cover the full Fe I Grotrian diagram quite well. The Oxford data include the lines modeled in detail by Lites and the lines of multiplets 41 and 43 above $\lambda = 400$ nm on which the outer part of the HOLMUL model is based.

b) Selection Effects

We display the input data in Fig. 2. The top panel shows the oscillator strengths of all lines against their upper-level excitation energy χ_u derived from the lower-level excitation energy χ_{exc} in MMH. Note that χ_u is a better discriminator than χ_{exc}, both for NLTE excitation departures (see Paper III) and for variation in collisional damping. The Kiev data in Fig. 2a (circles and crosses) show the selection effect that by using nice lines from the visual part of the spectrum one samples large oscillator strengths only of high-excitation lines. The low-excitation Oxford data (numbers) include lines of large oscillator strength, but these are mostly in the ultraviolet.

In Fig. 2b (bottom panel) we show the differences between the mean square radii Δr^2 of the upper and lower levels, one for each multiplet. Their variation exceeds two orders of magnitude! The radii are from the list by Warner (1969), who computed them from the scaled Thomas-Fermi formalism, taking care to include fractional parentage properly where necessary[1].

We have divided the Kiev data in Fig. 2a and b in lines and multiplets, respectively, with upper levels of even parity (crosses,

1 We draw attention to this useful compilation because it seems overly ignored, and because we believe that yet too often the ground-state ionization limit is erroneously used in computing the hydrogenic principal quantum numbers needed in all neutral-perturber damping formalisms

505 lines) and of odd parity (circles, 303 lines). All upper levels of the Oxford lines, indicated by their MMH multiplet number, are odd. This division illustrates Warner's (1967) explanation of the Carter (1949) effect, which is a parity split of the curve of growth. Figure 2b shows that it is identical to Warner's damping split, simply because the even upper levels happen to sample the large radii almost exclusively. The extensive study of the Carter split by Kuli-Zade et al. (1976) misses this point completely by ignoring Warner's work, and reaches a wrong conclusion.

Furthermore, Fig. 2b suggests that the practice of the Meudon group of dividing the damping part of the curve of growth in bins of lower-level excitation energy can be much improved by using bins of square radii difference (or upper-level radius) instead: while the maximum radius does increase with the excitation energy, the minimum does not, and at high excitation the whole range of radii is sampled.

Finally, Fig. 2 shows that the bin of lines with the largest damping contains also the high-excitation lines with the largest oscillator strengths. These lines probably have NLTE excitation departures that are not masked well by the HOLMUL model (see Paper III); if so, LTE fits of these lines, including their Kiev *gf* values, are suspect.

III. The Empirical Curve of Growth

a) Opacity Normalization

We now revert to a traditional Utrecht pastime and choose the curve of growth to display all lines simultaneously, employing its basic feature that it is a one-parameter representation which shows, all other things being or taken or made equal, the dependence of the observed line strength on the oscillator strength. Here, we comply with this spirit by eliminating the variations between lines that can be unambiguously accounted for, and then discuss the causes of the remaining variation.

The reason for the success of the concept "solar curve of growth" is that the contribution function to the equivalent width of a line peaks in about the same layer for lines of widely different strength. This is because the wings of strong lines, which contribute most to their equivalent widths, are like weak lines in formation: the trick of the curve of growth is to describe *all* lines as weak in formation. Assuming that the contribution functions are identical in location and shape leaves only their amplitude variation to be eliminated. In the classical curve of growth this is done through the term $-\chi_{\rm exc}\theta_{\rm exc}$ in the definition of the abscissa:

$$\log X = \log(gf\lambda A_{\rm Fe}) - \chi_{\rm exc}\theta_{\rm exc} + C\,, \qquad (1)$$

where f is the oscillator strength of a line, λ its wavelength, g the statistical weight of the lower level, $A_{\rm Fe} = N_{\rm Fe}/N_{\rm H}$ the iron abundance, $\chi_{\rm exc}$ the lower-level excitation energy, and $\theta_{\rm exc} = 5040/T_{\rm exc}$ the reciprocal excitation temperature, averaged over the layer of formation and assumed to be identical for all lines. The term $gf\lambda A_{\rm Fe}$ describes dependences of the line absorption coefficient. The term $-\chi_{\rm exc}\theta_{\rm exc}$ neutralizes the variation in line opacity due to the differences in Boltzmann population. The term C contains atomic constants.

More recent formulations (for a derivation see Jefferies, 1968, p. 276ff.) partially relax the assumption of a single, homogeneous layer of formation. The term C then contains the integral over the layer of formation of a weighting function which depends on the continuous absorption coefficient and on the continuum and line source functions. Sofar, LTE has been assumed in the computation of the weighting function, and the parameter $+\chi_{\rm ion}\theta_{\rm ion}$ describing the ionization equilibrium [see Jefferies (1968), Eq. (10.35)] has been ignored.

Here, we neutralize the variations in the opacities and in the source functions by explicit NLTE modeling. Our curve of growth is thus explicitly model dependent; but note that the choices of $\theta_{\rm exc}$ and C above are implicitly model dependent. In particular, we adopt the NLTE modeling of the solar Fe I spectrum by Athay and Lites (1972) and by Lites (1972, 1973), using Lites' results tabulated by Lites and White (1973) and summarized in Paper III. Fortunately, these show that the character of the Fe I NLTE departures should not inhibit the strategy of the curve of growth: in the deep layers where the weak lines and the wings of the strong lines are formed, all Fe I levels share identical height-dependent population departures (with the possible exception of the upper levels of the strongest high-excitation lines, for which the situation is not yet clear). One height-dependent NLTE correction to the populations should thus suffice for (almost) all Fe I lines.

In addition to admitting NLTE departures, we fully drop the assumption of a single layer of formation and admit variations in the location and shape of the contribution functions for weak lines. We do this by determining opacity normalization factors as functions of wavelength λ and excitation energy $\chi_{\rm exc}$. We derive these, for a grid spaced 100 nm in λ and 0.25 eV in $\chi_{\rm exc}$, by model computations in which a fictitious oscillator strength gf_6 is adjusted to produce a line strength $\log(W/\lambda) = -6$. We use the same computer program as in Paper III, and again adopt the atmospheric model given by Lites (1972, 1973; called LITES), which equals the HSRA (Gingerich et al., 1968) in the deep layers relevant here. The height-dependent microturbulence specified by Lites is, however, slightly modified, to which point we return in Sect. IV where we also specify the damping formalisms employed; the latter do not affect the computed weak-line opacity factors. For the NLTE departures we use Lites' height-dependent coefficients for the a^3F and z^5G^0 levels as representative lower- and upper-level departure coefficients. They are shown in Fig. 3b of Paper III; the corresponding wavelength-dependent NLTE excitation temperatures are shown in Fig. 4 of Paper III.

At short wavelengths the problem arises of the unknown opacity contribution by the line haze. We multiply the continuous opacity computed without line haze opacity by 1.05 at $\lambda = 500$ nm and by 1.14 at $\lambda = 400$ nm to obtain the reductions in continuum intensity given by Holweger (1970, respectively, 2.5 % and 8 %), and by 2 at $\lambda = 300$ nm to obtain the hazed "continuum" intensity given by Vernazza et al. (1981, their Fig. 26).

The differences in the fitted oscillator strengths gf_6 specify corrections that, when applied to the line opacity, offset variations with λ and $\chi_{\rm exc}$ as measured by the line strength for weak lines. These opacity corrections neutralize not only changes in line strength that are due to variations of the line and continuum opacities, but also changes due to variations of the line and continuum source functions. The concomitant abscissa for our curve of growth is:

$$\log X = \log gf - (\log gf_6 + 6)\,. \qquad (2)$$

The opacity normalization factors gf_6 are proportional to the inverse of the iron abundance used in the program; its value ($A_{\rm Fe} = 4.7\,10^{-5}$) was determined by requiring that the empirical curve of growth, discussed in the next section, has $\log X = \log(W/\lambda)$ for its Doppler part.

Table 1. Values of log gf_6, where gf_6 is the computed opacity normalization factor, as function of wavelength λ (nm) and lower-level excitation energy χ_{exc} (eV)

χ_{exc} \ λ	300	400	500	600	700	800
0.00	−6.6054	−6.7238	−6.7392	−6.7421	−6.7357	−6.7335
0.25	−6.3574	−6.4770	−6.4905	−6.4919	−6.4844	−6.4812
0.50	−6.1105	−6.2314	−6.2429	−6.2427	−6.2339	−6.2298
0.75	−5.8645	−5.9867	−5.9961	−5.9944	−5.9842	−5.9792
1.00	−5.6196	−5.7435	−5.7508	−5.7471	−5.7359	−5.7298
1.25	−5.3757	−5.5014	−5.5063	−5.5009	−5.4883	−5.4810
1.50	−5.1329	−5.2605	−5.2629	−5.2556	−5.2416	−5.2332
1.75	−4.8911	−5.0207	−5.0206	−5.0113	−4.9961	−4.9863
2.00	−4.6503	−4.7823	−4.7796	−4.7680	−4.7513	−4.7402
2.25	−4.4107	−4.5450	−4.5396	−4.5259	−4.5078	−4.4950
250	−4.1722	−4.3091	−4.3009	−4.2847	−4.2652	−4.2530
2.75	−3.9348	−4.0744	−4.0632	−4.0445	−4.0237	−4.0120
3.00	−3.6983	−3.8410	−3.8268	−3.8052	−3.7833	−3.7706
3.25	−3.4629	−3.6091	−3.5916	−3.5667	−3.5438	−3.5312
3.50	−3.2287	−3.3784	−3.3576	−3.3332	−3.3054	−3.2925
3.75	–	−3.1491	−3.1249	−3.1006	−3.0681	−3.0536
4.00	–	−2.9212	−2.8935	−2.8677	−2.8318	−2.8156
4.25	–	−2.6946	−2.6633	−2.6360	−2.5969	−2.5814
4.50	–	−2.4694	−2.4344	−2.4056	−2.3627	−2.3454
4.75	–	−2.2457	−2.2067	−2.1765	−2.1297	−2.1104
5.00	–	–	−1.9805	−1.9465	−1.8976	−1.8781
5.25	–	–	−1.7552	−1.7203	−1.6666	−1.6465
5.50	–	–	–	−1.4930	−1.4383	−1.4152
5.75	–	–	–	−1.2702	−1.2113	−1.1846
6.00	–	–	–	–	−0.9846	−0.9555
6.25	–	–	–	–	–	−0.7296

The resulting opacity normalization factors are listed in Table 1 and shown in Fig. 3a. The graphs show $\log gf_6 + 6 - \chi_{exc}$ against χ_{exc}. The curves would be displaced vertically if a different abundance were adopted. The subtraction by χ_{exc} enables comparison with the classical Boltzmann factor $-\chi_{exc}\theta_{exc}$ present in Eq. (1). The curves would be straight if a single mean excitation temperature θ_{exc} would suffice, and constant if $\theta_{exc}=1$. The actual curves are curved, from a slope corresponding to $\theta_{exc}\approx 1.0$ at $\chi_{exc}=0$ eV to a slope corresponding to $\theta_{exc}\approx 0.92$ at the highest excitation energy, because higher-excitation lines of equal strength are formed deeper in the atmosphere.

In addition, the curves and their slopes vary with wavelength, but only slightly. The differences in slope are due to the decrease with wavelength of the temperature sensitivity of the Planck function. The longer-wavelength curves nearly coincide at low excitation energy. The upward shifts of the short-wavelength curves are set by the line-haze fudge factors; for non-fudged continuous intensities we obtain the dashed curves. The line-haze addition results in upward shifts because a line for which the continuum is formed higher in the atmosphere requires a larger fictitious oscillator strength gf_6 to reach the strength $\log(W/\lambda)=-6$, due to the decrease of the gradient $|dB/d\tau|$ with height.

The near-equality of the curves near $\chi_{exc}=0$ eV contradicts the shift predicted by the classical term $+\log\lambda$ in Eq. (1), which differs by 0.43 between $\lambda=300$ nm and $\lambda=800$ nm. Proper derivation of the curve of growth (e.g. Mihalas, 1978, p. 316ff.) shows that the Doppler part has

$$W/\lambda \sim \eta_0,$$

where η_0 is the ratio of the line absorption coefficient to the continuous absorption coefficient at line center. The line absorption coefficient increases linearly with wavelength but the continuous absorption coefficient, which is dominated by H^-, also increases nearly linearly with wavelength throughout the visual, resulting in cancellation of the wavelength sensitivity of η_0.

Figure 3a shows the weak-line opacity factors for the NLTE LITES model, while Fig. 3b shows the results of a similar computation in which the NLTE departure coefficients were replaced by unity at all heights. The differences measure the effect on the equivalent width of neglecting the opacity reduction due to NLTE over-ionization. They are small for the deeply-formed high-excitation lines, and increase to 0.15 dex near $\chi_{exc}=0$ eV, implying equal corrections to the iron abundance determined from such lines which are a little larger than Holweger's (1973) estimate of $\leqq 0.1$ dex. Note that these solar NLTE corrections are much smaller than the laboratory NLTE corrections affecting the older experimental Fe I *gf*-values.

Figure 3a and b show that NLTE modeling as well as wavelength- and excitation-dependent computation of full contribution functions are required to define the abscissa of the curve of growth with better than 0.1 dex (25%) precision. However, a numerically adequate shortcut is provided by replacing the NLTE modeling by the assumption of the LTE HOLMUL photosphere.

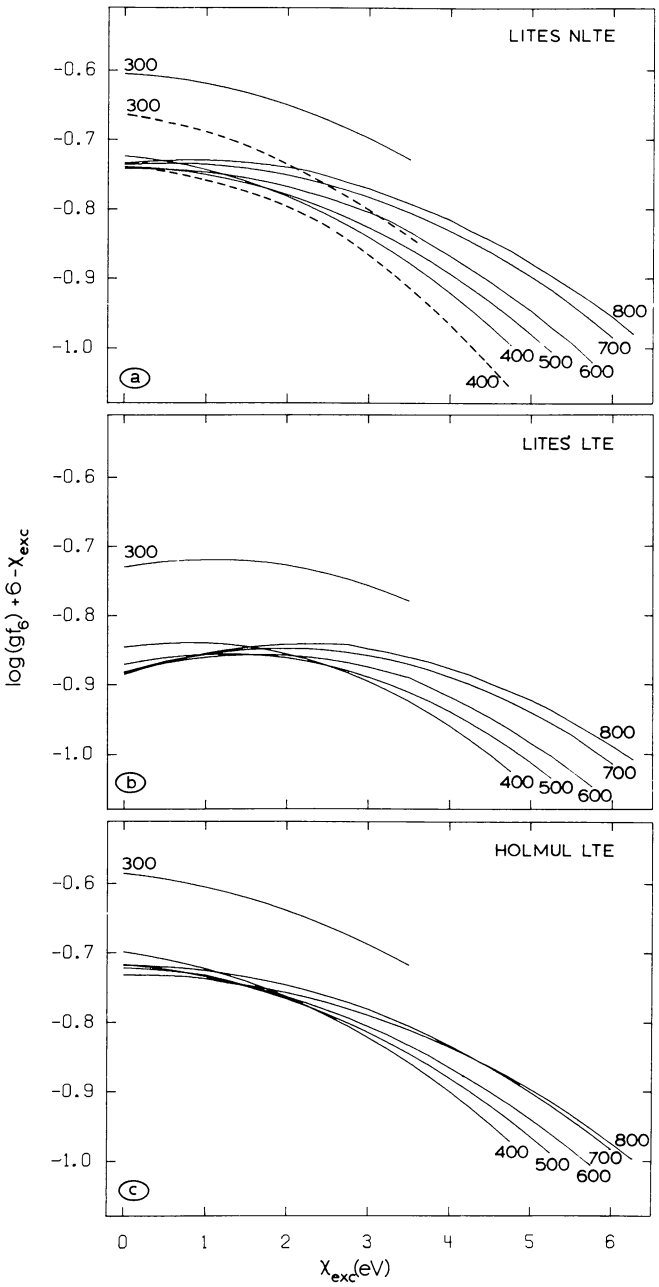

Fig. 3a–c. Opacity normalization curves for three models. The curves show the behaviour of $\log gf_6+6-\chi_{exc}$ against the lower-level excitation energy χ_{exc} for different wavelengths, specified in nm along the curves. The oscillator strength gf_6 is the one needed to obtain a line of the given wavelength and excitation energy with strength $\log(W/\lambda)=-6$. The top panel shows the NLTE results used in this paper. The dashed curves are the results obtained when the additional line-haze opacity is neglected. The middle and bottom panels show LTE results, respectively, for the LITES and for the HOLMUL models of the atmosphere. The close correspondence of the HOLMUL results with the NLTE LITES rather than with the LTE LITES results illustrates the effective NLTE-masking by the HOLMUL model

This is shown by Fig. 3c, which presents the results of a similar LTE computation with the HOLMUL model, adopting a height-independent microturbulence of $1\,km\,s^{-1}$ following Holweger et al. (1978). *The* HOLMUL *results are much closer to the* NLTE LITES *results, from which they deviate only* 0.02 dex *at most, then they are to the* LTE LITES *results!* This illustrates the conclusion of Paper III that the HOLMUL model effectively masks NLTE ionization departures for a wide variety of Fe I lines.

b) The NLTE *Curve of Growth*

Figure 4a shows the curve of growth obtained by plotting $\log(W/\lambda)$ against $\log X=\log gf-(\log gf_6+6)$. The opacity normalization term $-(\log gf_6+6)$ was found for each line by two-dimensional cubic spline interpolation in the results of Table 1. All lines were used; the Kiev and Oxford lines are drawn as dots and crosses, respectively. The triangles (top panel only) are Kiev lines with $\lambda>550$ nm, $\chi_{exc}>5$ eV and $\log gf>-1.0$. These long-wavelength lines of large transition probability are the ones of which the formation is yet in discussion (see Paper III); they probably have NLTE excitation departures that are not fully masked by the HOLMUL model, and their Kiev gf values are therefore dubious.

The initial results were used to set the iron abundance used in the gf_6 computations by determining the horizontal offset between a least-square polynomial fit of fifth order to the empirical curve and the line $\log(W/\lambda)=\log X$, at $\log(W/\lambda)=-6$. There are no additional shifts applied, not between the two data sets nor per multiplet; this type of empirical curve of growth has been termed 'absolute' before. The polynomial fit obtained is:

$$\log(W/\lambda)=-3.308+0.2044\,X-0.44866\,X^2-0.21725\,X^3 -0.036954\,X^4-0.0020118\,X^5\,.$$

The scatter around the mean curve is smaller than in previous investigations; its vertical standard deviation is 0.08 dex. The improvement due to the explicit computation of the opacity normalization factor per line is demonstrated through comparison with Figs. 4b and 4c, where traditional opacity factors are used for the same oscillator strengths. The curve of growth shown in Fig. 4b has as abscissa $\log X=\log gf\lambda-0.98\chi_{exc}$ following Cowley and Cowley's (1964) evaluation of Eq. (1), while the bottom curve (Fig. 4c) has $\log X=\log gf-1.09\chi_{exc}$ following Blackwell and Shallis (1979). In both cases the dashed lines mark the vertical 90% confidence limits per sample of the top curve, found from the fifth-order polynomial fit to all lines. The top curve has appreciably smaller spread than the other two. This shows that actual solar lines confirm our inference from Fig. 3 that better than 0.1 dex precision requires explicit modeling.

In addition, both traditional curves show distortion compared with the top curve. The population factor $\theta_{exc}=0.98$ of the Cowley and Cowley abscissa agrees well with the mean slope of the opacity curves of Fig. 3a, but its factor $\log\lambda$ results in selection skewness: the strongest lines lie in the violet and have smaller $\log\lambda$ offsets, while the weakest lines lie mostly in the red and have larger $\log\lambda$ offsets. The resulting curve of growth is compressed. The Blackwell and Shallis abscissa has no wavelength offsets, but its overly large population factor $\theta_{exc}=1.09$ produces leftward shifts of the high-excitation Kiev lines; the resulting curve of growth is expanded.

The scatter in the top curve increases somewhat towards both ends. The increase for the weakest lines is due to increasing uncertainty of the MMH equivalent widths since the MMH 0.1 Fraunhofer discretization becomes apparent below $\log(W/\lambda)\approx-5.7$. The increase for the strongest lines should not be due to uncertainties in oscillator strengths because the Oxford

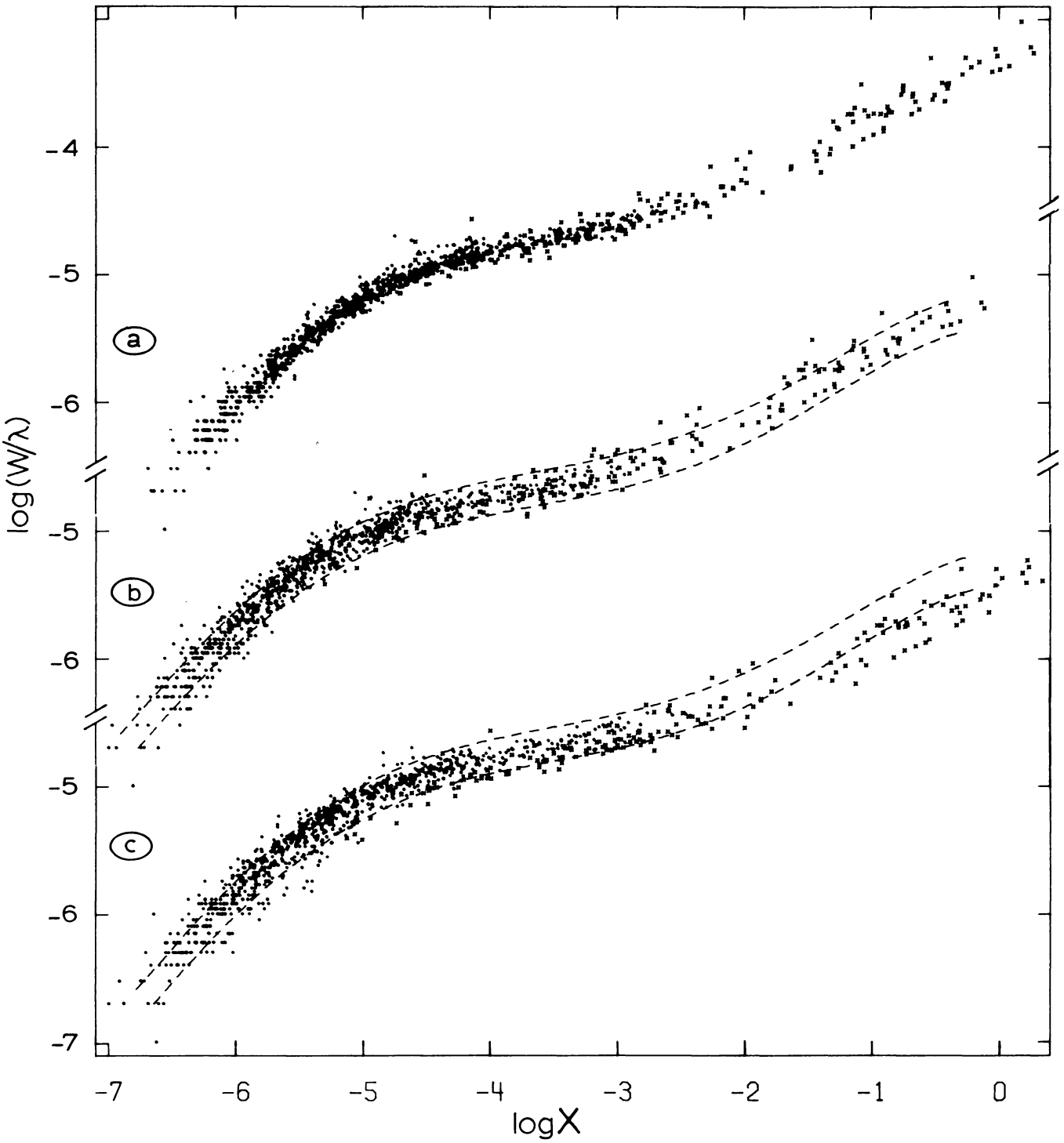

Fig. 4a–c. Empirical solar Fe I curves of growth for 991 lines, based on three different population normalization formalisms. The top curve is the NLTE result of this paper; its abscissa is $\log X = \log gf - (\log gf_6 + 6)$. The x-axis labeling belongs to this abscissa. The Kiev lines are shown as dots and triangles, and the Oxford lines are shown by crosses. The middle and bottom curves are for the classical abscissae defined in the text. They have been shifted horizontally to obtain a best fit at $\log(W/\lambda) = -6$ within the 90% confidence limits per sample of the top curve, which are shown by the overlaid dashed lines

group claims 1% (0.004 dex) relative accuracy; this is the topic of Sect. V.

The Kiev and Oxford data agree very well where they overlap (from $\log X = -5.0$ to $\log X = -2.5$): separate least-square polynomial fits to the two data sets are virtually identical in this range.

c) Comparison with Earlier Results

In Fig. 5 we compare the empirical curve of growth of Fig. 4a with earlier standards. The often-quoted curve by Cowley and Cowley (1964) is a composite curve of growth for lines of seven elements,

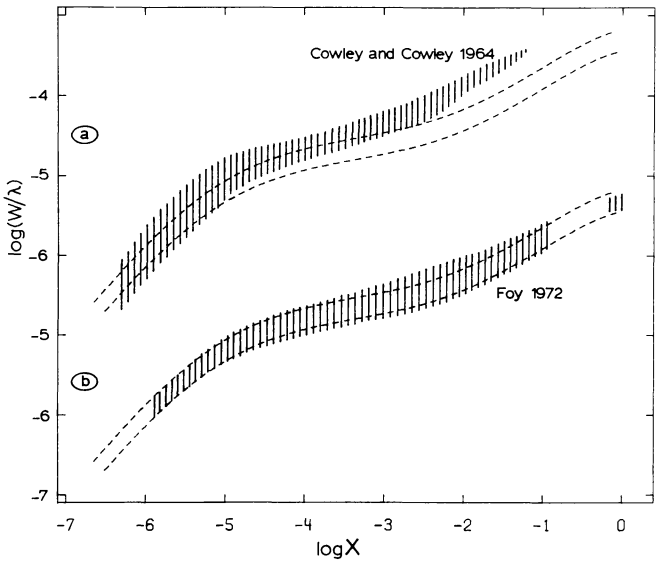

Fig. 5a and b. Comparison of the empirical NLTE curve of growth with earlier results. The dashed curves are the 90% confidence limits per sample of the curve of growth of Fig. 4a. The shaded areas are eye estimates of similar limits for the curves of Cowley and Cowley (1964, top) and Foy (1972, bottom). They have been shifted horizontally to obtain a best fit at $\log(W/\lambda) = -6$

based on the Corliss and Bozman (1962) oscillator strengths. It is compressed to a much larger extent than caused by the selective $\log\lambda$ skewing shown in Fig. 4b, illustrating deficiencies of the older gf-values.

The Fe I curve of growth of Foy (1972) in Fig. 5b is based on various newer sets of Fe I oscillator strengths brought together on the scale of Wolnik et al. (1970, 1971), and has an abscissa based on LTE weighting-function computations. Foy's curve is in better agreement with ours; its lower limit is nearly identical to the lower limit of our curve, but its higher limit rises appreciably above ours between $\log X = -4$ and $\log X = -1$.

IV. Theoretical Curves of Growth

a) Computations

In order to interpret the shape and the spread of the empirical curve of growth shown in Fig. 4a, we need theoretical predictions for comparison. We derive these by computing line profiles as a function of oscillator strength and plotting their strengths against $\log X$ from Eq. (2), again finding the opacity normalization $-(gf_6+6)$ through double interpolation in the results of Table 1. We thus reproduce the empirical procedure.

We adopt Lites' modeling as described above. For the damping we use the classical formula for van der Waals broadening [Unsöld (1955), Eq. (82.48)]

$$\gamma_{\mathrm{vdW}} = 17.0 \times 1.04 \times (6.46\,10^{-34}\Delta r^2)^{0.4}(2.16\,10^{8})^{0.3} N_{\mathrm{H}} T_e^{0.3},$$

where γ_{vdW} is the full halfwidth of the Lorentz profile in rad s^{-1}, N_{H} is the atomic hydrogen density per cm^3, T_e the electron temperature, and where the helium abundance is taken 0.1. The program adds classical radiation damping, quadratic Stark broadening and quadrupole electron broadening, but we do not specify these here because they are negligible. The initial results showed that the steep inward increase of the microturbulent velocity given by Lites results in too high a location of the plateau of the theoretical curve. We therefore replaced it by the less steep increase of the VALIII-C microturbulence model (Vernazza et al., 1981), maintaining Lites' model above $h = 300$ km (corresponding to $h = 2$ km in Lites' shifted "eclipse" height scale). The changed part does not affect the strong lines modeled by Lites. The opacity normalization curves of Fig. 3a were also computed with this microturbulence, and both the empirical and theoretical curves of growth have $\log(W/\lambda) = \log X$ for their Doppler parts, at all wavelengths and excitation energies.

Results are shown in Fig. 6. All curves have maximum oscillator strength $gf = 5$, so that the locations of their right-hand endings are set by the Boltzmann population and depend only on excitation energy. Only low-excitation lines reach the damping part. The visual lines with the largest transition probabilities present in the Kiev data are all at high excitation (Fig. 2a) and reach only up to the plateau part, as indeed shown empirically by Fig. 4. The dashed curves are again the 90% confidence limits per sample of the empirical curve of growth in Fig. 4a. Each set of curves contains the same "standard" curve, representing an average of the empirical data, with $\lambda = 550$ nm, $\chi_{\mathrm{exc}} = 1.5$ eV, $\Delta r^2 = 5$ a.u. and Lites' NLTE departure coefficients for the a^3F and z^5G^0 levels of his "ground term" model atom.

b) Sensitivity to Wavelength and Damping

The theoretical curves shown in Fig. 6a show a wavelength forking in the plateau part. This is due to the wavelength dependence of the line strength W/λ, which varies along the curve. The Doppler part has no wavelength dependence because it is explicitly neutralized by the gf_6 opacity normalization factors. The shoulder part, however, is forked because profile saturation is reached sooner, for increasing η_0, at longer wavelengths due to the smaller temperature sensitivity of the Planck function; the saturation depth of a line profile is smaller in the red part of the spectrum. The damping part has (see Mihalas, 1978, p. 320):

$$W/\lambda \sim (a\eta_0)^{1/2},$$

where the damping parameter $a = \gamma/(4\pi\Delta\nu_D)$ increases linearly with wavelength. The wavelength forking is therefore reversed at the start of the damping part; Fig. 6a shows that this results in near-cancellation of the wavelength dependence.

The more familiar damping forking is shown in Fig. 6b for the full range of square radii differences present in Fig. 2b. The split is indeed too large to be ignored.

c) Constant Microturbulence and Damping

The theoretical curves of Fig. 6a and b are based on comprehensive height-dependent modeling, whereas in classical analyses single height-independent values are assigned not only to the excitation temperature but also to the Doppler width and the damping constant. The first varies in our computations by a factor of two through the photosphere, the second by two orders of magnitude. For comparison we have computed curves of growth with height-independent microturbulence and damping. We find that the constant microturbulence of 1.0 km s^{-1} advised by Holweger et al. (1978) produces curves nearly identical to those of Fig. 6a, and that a choice of $a = 0.008$, 0.014, 0.023, and 0.056, respectively, reproduces the curves of Fig. 6b. Thus, the curve of

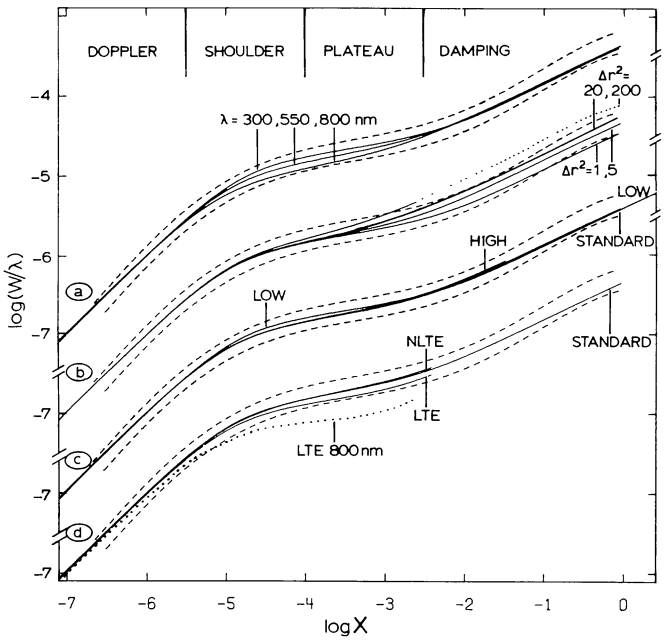

Fig. 6a–d. Comparison of the empirical curve of growth with various theoretical ones. The dashed curves mark the 90% confidence limits per sample of the empirical curve of Fig. 4a. The solid curves are theoretical curves of growth computed for different wavelength, damping and NLTE excitation. **a** Standard departure coefficients, $\chi_{exc}=1.5$ eV, $\Delta r^2=5$ a.u., $\lambda=300$, 550, and 800 nm as indicated. **b** Standard departure coefficients, $\lambda=550$ nm, $\chi_{exc}=1.5$ eV, $\Delta r^2=1$, 5, 20, and 200 a.u. as indicated. The $\Delta r^2=200$ a.u. curve is dotted where no actual lines are present. **c** and **d** Different upper-level departure coefficients, see text

growth is not a sensitive diagnostic to the height dependence of either parameter. Note that the maximum predicted damping is less than Foy's (1972) result $a\approx 0.08$ for many lines.

d) Sensitivity to NLTE *Excitation*

We turn now to the effects of NLTE departures in the excitation equilibrium. The question is not whether these exist (which is amply demonstrated by the observation that no Fe I line has a self-reversed emission core), but whether there is noticeable variation in line strength due to *differences* in the excitation departures between different lines. This we test in Fig. 6c by computing curves of growth for the extremes in the departure tabulation of Lites and White (1973). The "low" curve is for a $\lambda=400$ nm, $\chi_{exc}=0$ eV line with Lites' "ground term" model atom departure coefficients of a^5d and of z^5F^0, representative of strong low-excitation lines. The "high" curve is for a $\lambda=550$ nm, $\chi_{exc}=3.0$ eV line with the z^7P^0 and e^7D departure coefficients of Lites' "magnetic lines" model atom, representing the strongest high-excitation lines. The z^7P^0 level is one of the special levels named "metastable" by Athay and Lites, with downward lines of low transition probability only. The damping was computed from $\Delta r^2=5$ a.u. for all three curves. The curves (Fig. 6c) are virtually *identical*, except for the small split in the shoulder and plateau parts which is entirely due to the 400–550 nm wavelength difference. Thus, Lites' modeling predicts that *there are no differences whatsoever* in the curve of growth due to differences in NLTE excitation. This conclusion implies confirmation of the curve-of-growth strategy for even the strongest Fe I lines, and rejection of NLTE differences as a cause for the observed scatter in the damping part.

Finally, Fig. 6d shows that NLTE effects *may* be affecting the plateau part if we question Lites' modeling for high levels, as has been done (e.g. Ruland et al., 1980; see discussion in Paper III). The standard curve is again shown; the other solid curves are for high-excitation lines with $\lambda=550$ nm, $\chi_{exc}=4.0$ eV, $\Delta r^2=5$ a.u. and Lites' z^5G^0 departure coefficient assumed for the *lower* level. For the upper level Lites' e^7D coefficient is used for the curve labeled "NLTE", while it is replaced by unity throughout the atmosphere for the curve labeled "LTE". The first is representative of upper levels that are dominated by line photon losses rather deep in the photosphere, as are the examples computed by Lites and by Athay and Lites. The second is representative for upper levels that are strongly coupled to the Fe II ground state. They are the extremes of the possibilities discussed in Paper III. Figure 6d shows that the higher excitation temperature of the "LTE" case results in smaller line strength for lines with oscillator strength above $gf\approx 0.05$. The offset from the standard curve is largest for lines in the red; the dotted curve shows this for a similar $\lambda=800$ nm "LTE" line. (It is shifted away from the standard curve in the Doppler part because the change in upper-level population slightly affects the normalization factor which was not recomputed.) A similar computation for a $\lambda=400$ nm "LTE" line (not shown) gives a curve of growth close to the standard curve.

V. Comparison of Empirical and Theoretical Curves of Growth

a) The Fit of the Mean Curve of Growth

A comparison of the various theoretical curves of growth in Fig. 6 with the overlaid 90% confidence limits of the empirical curve shows that there is good overall agreement. All forkings are contained within the empirical spread, except for the trial $\lambda=800$ nm "LTE" curve of Fig. 6d. Note that the $\Delta r^2=200$ a.u. curve of Fig. 6b exceeds the upper 90% confidence limit only in the dotted range where no actual lines are present, because all lines of large Δr^2 are at high excitation energy; all Oxford lines except multiplet 152 have $\Delta r^2<20$ as shown in Fig. 2b. This good agreement indicates that there are no large distortions in the Oxford and Kiev oscillator strengths, and confirms that Lites' modeling applies also to the weak Fe I lines.

b) The Spread in the Empirical Curve of Growth

The empirical curve of growth shown in Fig. 4a should exhibit the forkings present in the theoretical curves of growth in Fig. 6. The observed spread, however, exceeds the theoretical forkings of the Doppler and damping parts; the vertical range between the 90% confidence limits is 0.3 dex and the vertical standard deviation is 0.08 dex along the whole curve. To analyze this spread we now split the curve of growth into the four parts labeled Doppler, shoulder, plateau and damping in Fig. 6, and we show in Fig. 7 the horizontal deviations $\Delta X=\log X_s-\log X$ for each line of each part from the standard $\lambda=550$ nm theoretical curve of Fig. 6a. The value $\log X_s$ is the abscissa value at which the standard curve reaches the observed value of $\log(W/\lambda)$; ΔX is positive to the left of the standard curve. The differences are plotted in Fig. 7 as function of $\log\lambda$, $\log\Delta r^2$ and $\log gf$, respectively. The predicted forkings are indicated in the appropriate panels through solid curves estimated from Fig. 6. The Kiev lines are split into odd and

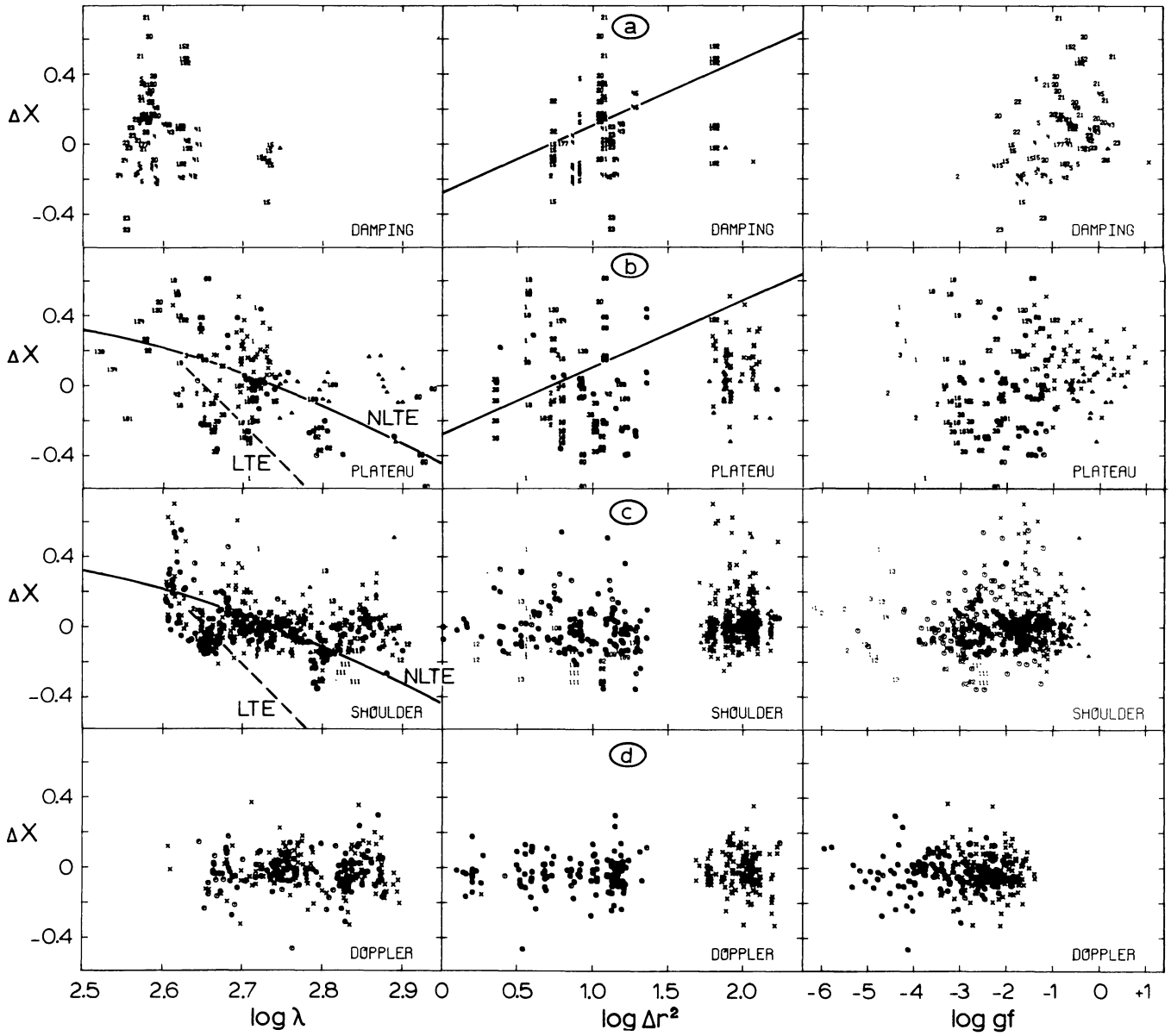

Fig. 7a–d. Scatter diagrams of the individual lines in the empirical curve of growth, split into the four parts defined in Fig. 6. The ordinate X measures the horizontal shift from an individual point in Fig. 4a to the standard $\lambda = 550$ nm theoretical curve of Fig. 6a, positive for points to the left of the standard curve. The solid and dashed lines are predictions based on Fig. 6. Crosses are Kiev lines with even-parity upper levels, circles are Kiev lines with odd-parity upper levels, triangles are Kiev lines with even-parity upper levels of which the gf values are suspect, numbers are the multiplet designations of the Oxford lines, which have odd-parity upper levels

even as in Fig. 2; the possibly deviating Kiev lines (with $\log gf > -1.0$, $\lambda > 550$ nm, $\chi_{exc} > 5.0$ eV) are shown by triangles.

We discuss these scatter diagrams part by part.

(i) The Damping Part

The damping part should be sensitive to Δr^2 only, because Fig. 6 shows negligible dependence on wavelength and none on NLTE excitation differences, and because the Oxford oscillator strengths are claimed to be highly accurate. Thus, the damping part should indeed obey Foy's assumption that all scatter is due to variation in damping only. One would expect the ΔX values to cluster tightly around the predicted line in the $\log \Delta r^2$ panel, or, if the assumption of van der Waals broadening is incorrect, to define a different but similar curve. The curve should be similar because the other formalisms for collisional broadening by neutral perturbers predict an increase with the hydrogenic principal quantum number of the upper level also.

In contrast to this expectation, Fig. 7a shows very large scatter in the Oxford lines, ranging over a full order of magnitude and over 0.7 dex *within* multiplets; it completely hides any systematic variation with Δr^2. The $\log \lambda$ panel indicates that this spread is largest for the ultraviolet lines, and we therefore attribute it to substantial errors in the MMH equivalent widths of these lines, arising from the severe line crowding present in this wavelength

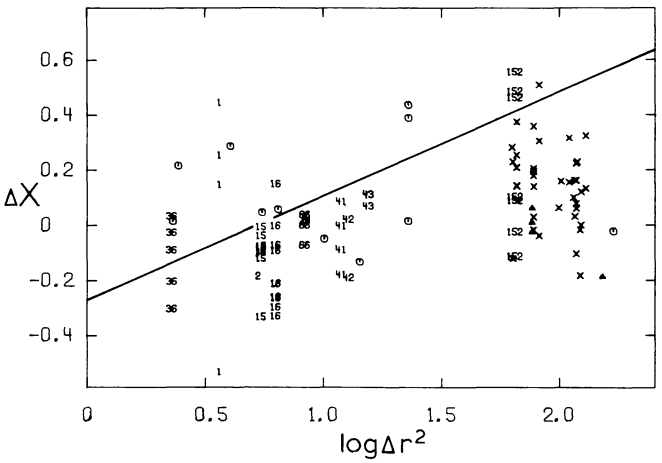

Fig. 8. Observed and predicted variation in collisional damping. Labeling as for the Δr^2 panels of Fig. 7, but for a selection of lines from the damping and plateau parts (see text) with small wavelength forking and better equivalent widths

region. Inspection of the Jungfraujoch Atlas (Delbouille et al., 1973) shows that most of the Oxford lines are traceable only in the inner cores, and that the locations of the local continua are highly uncertain. An experiment in which we integrated our own pencil-and-eye extrapolations of profiles in the Jungfraujoch Atlas yields indeed differences, both positive and negative, of up to 0.5 dex with the MMH equivalent widths. The suggestion given by the $\log gf$ panel of an increase of ΔX with oscillator strength within some multiplets may be due to systematic variations of these errors. The lines of multiplets 15, 41, 42, and 43 show smaller scatter and fit the predicted Δr^2 curve better. The two Kiev lines present (λ557.29 and λ538.34 nm) do not fit the relation, but these may have offsets discussed below.

(ii) The Plateau Part

The plateau part should have a mixture of ΔX values since it has predicted wavelength and damping forkings shown by solid curves in the $\log\lambda$ and $\log\Delta r^2$ panels, and possibly a NLTE-LTE forking for high-excitation lines of which the range is indicated by the curves in the $\log\lambda$ panel.

The spread (Fig. 7b) is again larger than the predicted forkings, especially for the ultraviolet Oxford lines. We attribute this again to MMH errors in the equivalent widths. For the Kiev lines the $\log\Delta r^2$ panel exhibits the Carter (1949) effect: the mean of the lines with odd upper levels (crosses and triangles) is higher than the mean of the lines with even upper levels (circles). The $\log gf$ panel shows this also, because of the selection effects displayed by Fig. 2.

The mean trend in the $\log\lambda$ panel follows the predicted wavelength dependence, shown by the solid curve. The long-wavelength lines contradict the trial "LTE" prediction (upper level coupled to the Fe II ground state), and favor the "NLTE" prediction (upper-level depopulation by photon losses) for high-excitation lines, which is also favored by the results in Fig. 6 of Paper III. However, we have to take into account, first, that the triangles are raised by the damping split, and secondly, that their Kiev oscillator strengths are derived from solar line depths and contain implicit corrections for such NLTE excitation differences, if present. If, as we suspect, the "NLTE" case is the correct one, the Kiev gf values for the strongest high-excitation lines are too large; thus, their ΔX values are too small. Figure 6 of Paper III shows that such corrections will not exceed 0.5 dex; they will not change our curve of growth by much because only the plateau part is affected. In particular, such leftward shifts of the triangles in Fig. 4a do not lead to reproduction of the high upper boundary of Foy's curve in Fig. 5b.

We conclude that the mixture of the wavelength forking, damping forking, oscillator strength uncertainties and equivalent width errors which affects the strong high-excitation lines makes the plateau part too confused to draw firm conclusions on the yet unsettled LTE-NLTE dichotomy regarding the excitation of these lines; this question remains therefore open. However, our curve of growth is not much affected by this uncertainty, as shown by the close agreement of the separate least-square fits to the Oxford and Kiev lines mentioned above.

Another question that we cannot settle from the curve of growth is the one of collisional damping. In Fig. 8 we combine the ΔX offsets of the lines of the damping part with $2.6 < \log\lambda$ and of the plateau part with $2.68 < \log\lambda < 2.75$, so taking out most of the line crowding and of the wavelength forking as sources of variation. Figure 8 displays the Carter parity split more clearly, and the average agreement in slope with the predicted curve confirms Warner's (1967) explanation. The van der Waals prediction seems to *exceed* the actual mean slightly, but we do not consider this result significant in view of the noise. With regard to the latter, we see no reason to ascribe the noise solely to the variation in collisional damping postulated by Foy (1972); we rather suggest that only detailed center-to-limb analysis of line profiles may provide the constraints to warrant such an hypothesis. Note that Lites, whose study is the single existing Fe I analysis of such sophistication, used Brückner's (1971) formalism and found it adequate.

(iii) The Shoulder Part

The predicted damping forking is negligible for the shoulder part, but the predicted wavelength forking and possible excitation differences are still present, varying in size from $\Delta X = 0$ up to the maxima indicated by the solid and dashed curves in Fig. 7c. The $\log\Delta r^2$ panel shows indeed no difference between the odd and even lines. The ΔX distribution shows no significant structure in this panel, nor in the $\log gf$ panel, except for an upward tail. This we attribute to overestimated MMH equivalent widths for blended lines, since the significant rise for lines with $\lambda < 500$ nm in the $\log\lambda$ panel corresponds to the increased line crowding in the blue. The long-wavelength lines favor the NLTE prediction, except for the curious dip near $\log\lambda = 2.8$. This dip is also present in the other $\log\lambda$ panels. In Fig. 9 we have combined these together in a single $\log\lambda$ plot for all lines. The dip seems significant, but we have no explanation for it. It sets in near $\lambda = 610$ nm and it peaks near $\lambda = 625$ nm. If it were due to telluric line blocking it should rather start and peak both at $\lambda = 628$ nm, where the O_2 absorption sets in.

(iv) The Doppler Part

The Doppler part is without any predicted forking. The observed scatter distributions confirm this expectation: no panel of Fig. 7d shows significant deviations from accidental errors. The standard deviation of 0.08 dex corresponds well with the error estimate of 0.07 dex by Gurtovenko and Kostik (1982) for their oscillator strengths.

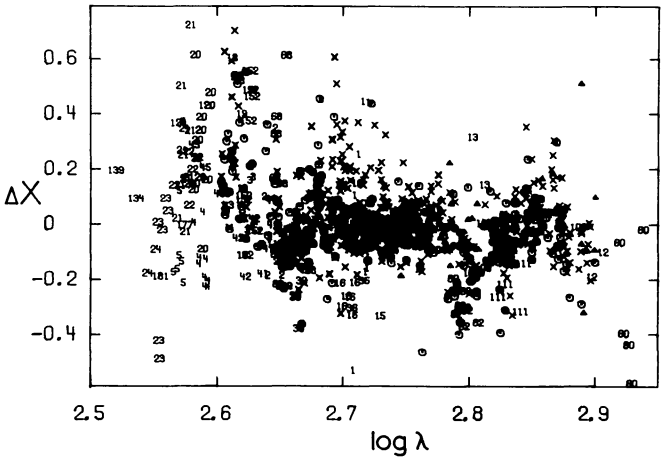

Fig. 9. Offsets ΔX of all 991 lines of the empirical curve of growth of Fig. 4a from the standard theoretical curve of growth, against wavelength. Labeling as for Fig. 7. The large spread below $\lambda = 450$ nm ($\log\lambda = 2.65$) is attributed to errors in the MMH equivalent width values due to the difficulty of defining line profiles and continua in the violet. The upward spread at longer wavelengths is attributed to neglected blends. The curious dip near $\log\lambda = 2.8$ is unexplained

VI. The Solar Iron Abundance

The predicted absence of forkings of the Doppler part and the observed absence of systematic deviations in the bottom panels of Fig. 7 justify our determination of the solar iron abundance through least-square fitting of the Doppler part to the line $\log(W/\lambda) = \log X$ at $\log(W/\lambda) = -6$. The result is: $A_{Fe} = N_{Fe}/N_H = 4.7\,10^{-5}$, or $A_{Fe}^{12} = 7.67$ on the $\log N_H = 12$ scale. The error in the fit is less than 0.02 dex, unless we underestimate the systematic error in the MMH equivalent widths or in the Oxford oscillator strengths. The quality of the MMH equivalent widths will be tested elsewhere (Rutten and van der Zalm, in preparation); the Oxford group claims an absolute accuracy of 0.01 dex.

The systematic error depends further on the appropriateness of Lites' modeling, used to compute the opacity normalization curves of Fig. 3a. Its error cannot be evaluated short of completely independent NLTE computations of at least similar sophistication; especially the amount of overionization due to the ultraviolet bound-free transitions is of interest here. However, these ionization departures cannot be very wrong in Lites' modeling, because the LTE HOLMUL model, which in essence constitutes a roundabout empirical determination of their size, agrees well (see Paper III). Taking the size of the differences between the HOLMUL LTE and the LITES NLTE opacity curves in Fig. 3 as indicator, we find that the systematic modeling error is also less than 0.02 dex. We therefore claim 10% accuracy for our abundance value, subject to a possible systematic correction of the MMH equivalent widths. A similar accuracy should be in reach of comparable stellar analyses, provided these include either estimation of the NLTE ionization balance, or fabrication of an HOLMUL-like NLTE-masking atmospheric model.

The most recent LTE determinations from Fe I lines agree with our result $A_{Fe}^{12} = 7.67 \pm 0.04$ if the HOLMUL model was adopted (e.g. Blackwell et al., 1980: $A_{Fe}^{12} = 7.69$), or they are smaller by about 0.1 dex if HSRA-like models were used (e.g. Biémont and Grevesse, 1975: $A_{Fe}^{12} = 7.57 \pm 0.11$), in agreement with the average NLTE-LTE difference in Fig. 3. Curiously, we find disagreement with Gurtovenko and Kostik's own value ($A_{Fe}^{12} = 7.57 \pm 0.01$) from the same data. Biémont's (1975) independent determination from Fe II lines agrees well ($A_{Fe}^{12} = 7.65 \pm 0.15$).

VII. Conclusions

The curve of growth remains useful to display the formation of many solar Fe I lines simultaneously, because the NLTE departures affecting the curve of growth are limited to the ionization departures in the deep photosphere, and affect all Fe I lines equally. Differences in excitation departures are probably only present for strong high-excitation lines, and hardly noticeable in the curve of growth. The wavelength dependences are small, and happen to cancel in the damping part. Our use of the curve of growth has led to confirmation of all conclusions of Paper III, to better recipes for stellar applications of the curve of growth, and to an improved value of the solar iron abundance.

We conclude from the scatter diagrams in Fig. 7 that the principal benefit of curves of growth remains the use of the Doppler part for abundance determinations. We attribute the large spread for the strongest lines primarily to errors in the MMH equivalent widths, rather than to the larger-than-predicted variation in damping postulated by Foy (1972), whose strong-line curve of growth we do not reproduce. The plateau part is too confused by its diverse forkings to be diagnostically useful.

The equivalent widths have now succeeded the oscillator strengths as major error source. Improvement of the equivalent width values of the strong lines requires extrapolation of line-core fits to obtain the wings, thus line core modeling of the consistency and complexity of Lites' NLTE modeling, based on as precise center-to-limb observations as used by him (Lites and Brault, 1972). Such modeling repudiates the strategy of the curve of growth, which is to avoid individual line synthesis. This strategy thus fails for interests other than abundance values; but such interests require more observational constraints anyhow. In particular, equivalent widths alone do not provide adequate diagnostics to discuss the merits of differing damping formalisms, atmospheric models, velocity fileds, or line-formation formalisms. Lites' detailed center-to-limb analysis of the profiles of many representative Fe I lines remains the outstanding example of combining the proper observational constraints with the proper modeling.

Acknowledgements. We are indebted to Jhr. H.J. Repelaer van Driel for punching the Oxford and Kiev data, and to Drs. A.A. van Ballegooijen and A. Schadee for comments on the manuscript.

References

Athay, R.G., Lites, B.W.: 1972, *Astrophys. J.* **176**, 809
Biémont, E.: 1978, *Monthly Notices Roy. Astron. Soc.* **184**, 683
Biémont, E., Grevesse, N.: 1975, *Solar Phys.* **45**, 59
Blackwell, D.E., Ibbetson, P.A., Petford, A.D., Shallis, M.J.: 1979, *Monthly Notices Roy. Astron. Soc.* **186**, 633
Blackwell, D.E., Petford, A.D., Shallis, M.J.: 1979, *Monthly Notices Roy. Astron. Soc.* **186**, 657
Blackwell, D.E., Shallis, M.J.: 1979, *Monthly Notices Roy. Astron. Soc.* **186**, 673

Blackwell, D.E., Shallis, M.J., Simmons, G.J.: 1980, *Astron. Astrophys.* **81**, 340
Blackwell, D.E., Petford, A.D., Shallis, M.J., Simmons, G.J.: 1980, *Monthly Notices Roy. Astron. Soc.* **191**, 445
Blackwell, D.E., Petford, A.D., Shallis, M.J., Simmons, G.J.: 1982, *Monthly Notices Roy. Astron. Soc.* **199**, 43
Brückner, K.A.: 1971, *Astrophys. J.* **169**, 621
Carter, W.W.: 1949, *Phys. Rev.* **76**, 962
Cayrel, G., Cayrel, R., Foy, R.: 1977, *Astron. Astrophys.* **54**, 797
Cayrel, R., Jugaku, J.: 1963, *Ann. Astrophys.* **26**, 495
Corliss, C.H., Bozman, W.R.: 1962, *Natl. Bur. St. U.S. Monograph* **53**, Washington
Cowley, C.R., Cowley, A.P.: 1964, *Astrophys. J.* **140**, 713
Delbouille, L., Roland, G., Neven, L.: 1973, Photoelectric Atlas of the Solar Spectrum from λ3000 to λ10,000, Inst. Astrophys. Liège
Foy, R.: 1972, *Astron. Astrophys.* **18**, 26
Gingerich, O., Noyes, R.W., Kalkofen, W., Cuny, Y.: 1971, *Solar Phys.* **18**, 347
Gurtovenko, E.A., Kostik, R.I.: 1981, *Astron. Astrophys. Suppl.* **46**, 239
Holweger, H.: 1970, *Astron. Astrophys.* **4**, 11
Holweger, H.: 1973, *Solar Phys.* **30**, 35
Holweger, H., Gehlsen, M., Ruland, F.: 1978, *Astron. Astrophys.* **70**, 537
Holweger, H., Müller, E.A.: 1974, *Solar Phys.* **39**, 19
Jefferies, J.T.: 1968, Spectral Line Formation, Blaisdell Publ. Co., Waltham
Kuli-Zade, D.M., Guseinov, K.I., Veliev, S.M.: 1976, *Soviet Astron.* **20**, 326 = *Astron. Zh.* **53**, 577
Lites, B.W.: 1972, NCAR Cooperative Thesis Nr. 28, Univ. Colorado High Altitude Observatory, Boulder
Lites, B.W.: 1973, *Solar Phys.* **32**, 283
Lites, B.W., Brault, J.W.: 1972, *Solar Phys.* **30**, 283
Lites, B.W., White, O.R.: 1973, High Altitude Observatory Research Memorandum No. 185, Boulder
Mihalas, D.: 1978, Stellar Atmospheres, 2nd ed., Freeman, San Francisco
Moore, Ch.E.: 1959, A Multiplet Table of Astrophysical Interest, *Natl. Bur. St. U.S. Techn. Note* **36**, Washington
Moore, Ch.E., Minnaert, M.G.J., Houtgast, J.: 1966, The Solar Spectrum 2935 Å to 8770 Å, *Natl. Bur. St. U.S. Monograph* **61**, Washington
Pagel, B.E.J.: 1965, Roy. *Observ. Bull. No.* 104
Ruland, F., Holweger, H., Griffin, R., Griffin, R., Biehl, D.: 1980, *Astron. Astrophys.* **92**, 70
Rutten, R.J., Kostik, R.I.: 1982, *Astron. Astrophys.* (in press, Paper III)
Unsöld, A.: 1955, Physik der Sternatmosphären, Springer, Berlin, Göttingen, Heidelberg
Vernazza, J.E., Avrett, E.H., Loeser, R.: 1981, *Astrophys. J. Suppl.* **45**, 350
Warner, B.: 1967, *Monthly Notices Roy. Astron. Soc.* **136**, 381
Warner, B.: 1969, *Observatory* **89**, 11
Wolnik, S.J., Berthel, R.O., Wares, G.W.: 1970, *Astrophys. J.* **162**, 1037
Wolnik, S.J., Berthel, R.O., Wares, G.W.: 1971, *Astrophys. J.* **166**, L 31
Yamashita, Y.: 1972, *Publ. Astron. Soc. Japan* **24**, 49

Note added in proof: During the session "Atomic and Molecular Data in Stellar Spectra" of the recent IAU General Assembly at Patras Dr. W. L. Wiese has shown that the values of the Kiev oscillator strengths are too large above $\log gf = -1.5$. The excesses increase with $\log gf$, continuing the trend suggested at right in Fig. 1.

This result confirms our interpretation of Fig. 6 of Paper III, and implies that the line source functions of the strongest high-excitation lines drop *below* the Planck function, in agreement with the predictions of Athay and Lites (1972) and Lites (1972). Thus, the "NLTE" prediction of Fig. 6d is indeed correct.